Prospects for Localization of Gravitational Wave Transients by the Advanced LIGO and Advanced Virgo Observatories

J. Aasi[1], J. Abadie[1], B. P. Abbott[1], R. Abbott[1], T. D. Abbott[2], M. Abernathy[3], T. Accadia[4], F. Acernese[5ac], C. Adams[6], T. Adams[7], P. Addesso[8], R. X. Adhikari[1], C. Affeldt[9,10], M. Agathos[11a], O. D. Aguiar[12], P. Ajith[1], B. Allen[9,13,10], A. Allocca[14ac], E. Amador Ceron[13], D. Amariutei[15], S. B. Anderson[1], W. G. Anderson[13], K. Arai[1], M. C. Araya[1], C. Arceneaux[16], S. Ast[9,10], S. M. Aston[6], P. Astone[17a], D. Atkinson[18], P. Aufmuth[10,9], C. Aulbert[9,10], L. Austin[1], B. E. Aylott[19], S. Babak[20], P. Baker[21], G. Ballardin[22], S. Ballmer[23], Y. Bao[15], J. C. Barayoga[1], D. Barker[18], F. Barone[5ac], B. Barr[3], L. Barsotti[24], M. Barsuglia[25], M. A. Barton[18], I. Bartos[26], R. Bassiri[3,27], M. Bastarrika[3], A. Basti[14ab], J. Batch[18], J. Bauchrowitz[9,10], Th. S. Bauer[11a], M. Bebronne[4], B. Behnke[20], M. Bejger[28c], M.G. Beker[11a], A. S. Bell[3], C. Bell[3], G. Bergmann[9,10], J. M. Berliner[18], A. Bertolini[9,10], J. Betzwieser[6], N. Beveridge[3], P. T. Beyersdorf[29], T. Bhadbade[27], I. A. Bilenko[30], G. Billingsley[1], J. Birch[6], S. Biscans[24], M. Bitossi[14a], M. A. Bizouard[31a], E. Black[1], J. K. Blackburn[1], L. Blackburn[32], D. Blair[33], B. Bland[18], M. Blom[11a], O. Bock[9,10], T. P. Bodiya[24], C. Bogan[9,10], C. Bond[19], F. Bondu[34b], L. Bonelli[14ab], R. Bonnand[35], R. Bork[1], M. Born[9,10], V. Boschi[14a], S. Bose[36], L. Bosi[37a], B. Bouhou[25], J. Bowers[2], C. Bradaschia[14a], P. R. Brady[13], V. B. Braginsky[30], M. Branchesi[38ab], J. E. Brau[39], J. Breyer[9,10], T. Briant[40], D. O. Bridges[6], A. Brillet[34a], M. Brinkmann[9,10], V. Brisson[31a], M. Britzger[9,10], A. F. Brooks[1], D. A. Brown[23], D. D. Brown[19], F. Brueckner[19], K. Buckland[1], T. Bulik[28b], H. J. Bulten[11ab], A. Buonanno[41], J. Burguet–Castell[42], D. Buskulic[4], C. Buy[25], R. L. Byer[27], L. Cadonati[43], G. Cagnoli[35,44], E. Calloni[5ab], J. B. Camp[32], P. Campsie[3], K. Cannon[45], B. Canuel[22], J. Cao[46], C. D. Capano[41], F. Carbognani[22], L. Carbone[19], S. Caride[47], A. D. Castiglia[48], S. Caudill[13], M. Cavaglià[16], F. Cavalier[31a], R. Cavalieri[22], G. Cella[14a], C. Cepeda[1], E. Cesarini[49a], T. Chalermsongsak[1], S. Chao[101], P. Charlton[50], E. Chassande-Mottin[25], X. Chen[33], Y. Chen[51], A. Chincarini[52], A. Chiummo[22], H. S. Cho[53], J. Chow[54], N. Christensen[55], Q. Chu[33], S. S. Y. Chua[54], C. T. Y. Chung[56], G. Ciani[15], F. Clara[18], D. E. Clark[27], J. A. Clark[43], F. Cleva[34a], E. Coccia[49ab], P.-F. Cohadon[40], C. N. Colacino[14ab], A. Colla[17ab], M. Colombini[17b], M. Constancio Jr.[12], A. Conte[17ab], D. Cook[18], T. R. Corbitt[2], M. Cordier[29], N. Cornish[21], A. Corsi[103], C. A. Costa[2,12], M. Coughlin[57], J.-P. Coulon[34a], S. Countryman[26], P. Couvares[23], D. M. Coward[33], M. Cowart[6], D. C. Coyne[1], K. Craig[3], J. D. E. Creighton[13], T. D. Creighton[44], A. Cumming[3], L. Cunningham[3], E. Cuoco[22], K. Dahl[9,10], M. Damjanic[9,10], S. L. Danilishin[33], S. D'Antonio[49a], K. Danzmann[9,10], V. Dattilo[22], B. Daudert[1], H. Daveloza[44], M. Davier[31a], G. S. Davies[3], E. J. Daw[58], T. Dayanga[36], R. De Rosa[5ab], G. Debreczeni[59], J. Degallaix[35], W. Del Pozzo[11a], E. Deleeuw[15], T. Denker[10], T. Dent[9,10], V. Dergachev[1], R. DeRosa[2], R. DeSalvo[8], S. Dhurandhar[60], L. Di Fiore[5a], A. Di Lieto[14ab], I. Di Palma[9,10], A. Di Virgilio[14a], M. Díaz[44], A. Dietz[4,16], F. Donovan[24], K. L. Dooley[9,10], S. Doravari[1], M. Drago[61ab], S. Drasco[20], R. W. P. Drever[62], J. C. Driggers[1], Z. Du[46], J.-C. Dumas[33], S. Dwyer[24], T. Eberle[9,10], M. Edwards[7], A. Effler[2], P. Ehrens[1], S. S. Eikenberry[15], G. Endrőczi[59], R. Engel[1], R. Essick[24], T. Etzel[1], K. Evans[3], M. Evans[24], T. Evans[6], M. Factourovich[26], V. Fafone[49ab], S. Fairhurst[7], Q. Fang[33], B. F. Farr[63], W. Farr[63], M. Favata[13], D. Fazi[63], H. Fehrmann[9,10], D. Feldbaum[15], I. Ferrante[14ab], F. Ferrini[22], F. Fidecaro[14ab], L. S. Finn[64], I. Fiori[22], R. P. Fisher[23], R. Flaminio[35], S. Foley[24], E. Forsi[6], L. A. Forte[5a], N. Fotopoulos[1], J.-D. Fournier[34a], J. Franc[35], S. Franco[31a], S. Frasca[17ab], F. Frasconi[14a], M. Frede[9,10], M. A. Frei[48], Z. Frei[65], A. Freise[19], R. Frey[39], T. T. Fricke[9,10], D. Friedrich[9,10], P. Fritschel[24], V. V. Frolov[6], M.-K. Fujimoto[66], P. J. Fulda[15], M. Fyffe[6], J. Gair[57], M. Galimberti[35], L. Gammaitoni[37ab], J. Garcia[18], F. Garufi[5ab], M. E. Gáspár[59], N. Gehrels[32], G. Gelencser[65], G. Gemme[52], E. Genin[22], A. Gennai[14a], L. Á. Gergely[67], S. Ghosh[36], J. A. Giaime[2,6], S. Giampanis[13], K. D. Giardina[6], A. Giazotto[14a], S. Gil-Casanova[42], C. Gill[3], J. Gleason[15], E. Goetz[9,10], G. González[2], N. Gordon[3], M. L. Gorodetsky[30],

S. Gossan[51], S. Goßler[9,10], R. Gouaty[4], C. Graef[9,10], P. B. Graff[32], M. Granata[35], A. Grant[3], S. Gras[24], C. Gray[18], R. J. S. Greenhalgh[68], A. M. Gretarsson[69], C. Griffo[70], H. Grote[9,10], K. Grover[19], S. Grunewald[20], G. M. Guidi[38ab], C. Guido[6], E. K. Gustafson[1], R. Gustafson[47], D. Hammer[13], G. Hammond[3], J. Hanks[18], C. Hanna[71], J. Hanson[6], K. Haris[72], J. Harms[62], G. M. Harry[73], I. W. Harry[23], E. D. Harstad[39], M. T. Hartman[15], K. Haughian[3], K. Hayama[66], J. Heefner[1], A. Heidmann[40], M. C. Heintze[6], H. Heitmann[34a], P. Hello[31a], G. Hemming[22], M. A. Hendry[3], I. S. Heng[3], A. W. Heptonstall[1], M. Heurs[9,10], M. Hewitson[9,10], S. Hild[3], D. Hoak[43], K. A. Hodge[1], K. Holt[6], M. Holtrop[74], T. Hong[51], S. Hooper[33], J. Hough[3], E. J. Howell[33], V. Huang[101], E. A. Huerta[23], B. Hughey[69], S. H. Huttner[3], M. Huynh[13], T. Huynh–Dinh[6], D. R. Ingram[18], R. Inta[54], T. Isogai[24], A. Ivanov[1], B. R. Iyer[75], K. Izumi[66], M. Jacobson[1], E. James[1], H. Jang[76], Y. J. Jang[63], P. Jaranowski[28d], E. Jesse[69], W. W. Johnson[2], D. Jones[18], D. I. Jones[77], R. Jones[3], R.J.G. Jonker[11a], L. Ju[33], P. Kalmus[1], V. Kalogera[63], S. Kandhasamy[78], G. Kang[76], J. B. Kanner[32], M. Kasprzack[22,31a], R. Kasturi[79], E. Katsavounidis[24], W. Katzman[6], H. Kaufer[9,10], K. Kawabe[18], S. Kawamura[66], F. Kawazoe[9,10], D. Keitel[9,10], D. Kelley[23], W. Kells[1], D. G. Keppel[9,10], A. Khalaidovski[9,10], F. Y. Khalili[30], E. A. Khazanov[80], B. K. Kim[76], C. Kim[76], K. Kim[81], N. Kim[27], Y. M. Kim[53], P. J. King[1], D. L. Kinzel[6], J. S. Kissel[24], S. Klimenko[15], J. Kline[13], K. Kokeyama[2], V. Kondrashov[1], S. Koranda[13], W. Z. Korth[1], I. Kowalska[28b], D. Kozak[1], C. Kozameh[82], A. Kremin[78], V. Kringel[9,10], B. Krishnan[10,9], A. Królak[28ae], C. Kucharczyk[27], G. Kuehn[9,10], P. Kumar[23], R. Kumar[3], B. J. Kuper[70], R. Kurdyumov[27], P. Kwee[24], M. Landry[18], B. Lantz[27], P. D. Lasky[56], C. Lawrie[3], A. Lazzarini[1], A. Le Roux[6], P. Leaci[20], C. H. Lee[53], H. K. Lee[81], H. M. Lee[83], J. Lee[70], J. R. Leong[9,10], N. Leroy[31a], N. Letendre[4], B. Levine[18], V. Lhuillier[18], T. G. F. Li[11a], A. C. Lin[27], V. Litvine[1], Y. Liu[46], Z. Liu[15], N. A. Lockerbie[84], D. Lodhia[19], K. Loew[69], J. Logue[3], A. L. Lombardi[41], M. Lorenzini[49ab], V. Loriette[31b], M. Lormand[6], G. Losurdo[38a], J. Lough[23], M. Lubinski[18], H. Lück[9,10], A. P. Lundgren[9,10], J. Macarthur[3], E. Macdonald[7], B. Machenschalk[9,10], M. MacInnis[24], D. M. Macleod[7], F. Magana-Sandoval[70], M. Mageswaran[1], K. Mailand[1], E. Majorana[17a], I. Maksimovic[31b], V. Malvezzi[49a], N. Man[34a], G. Manca[20], I. Mandel[19], V. Mandic[78], M. Mantovani[14a], F. Marchesoni[37ac], F. Marion[4], S. Márka[26], Z. Márka[26], A. Markosyan[27], E. Maros[1], J. Marque[22], F. Martelli[38ab], I. W. Martin[3], R. M. Martin[15], D. Martonov[1], J. N. Marx[1], K. Mason[24], A. Masserot[4], F. Matichard[24], L. Matone[26], R. A. Matzner[85], N. Mavalvala[24], G. May[15], G. Mazzolo[9,10], K. McAuley[29], R. McCarthy[18], D. E. McClelland[54], S. C. McGuire[86], G. McIntyre[1], J. McIver[43], G. D. Meadors[47], M. Mehmet[9,10], J. Meidam[11a], T. Meier[10,9], A. Melatos[56], G. Mendell[18], R. A. Mercer[13], S. Meshkov[1], C. Messenger[7], M. S. Meyer[6], H. Miao[51], C. Michel[35], L. Milano[5ab], J. Miller[54], Y. Minenkov[49a], C. M. F. Mingarelli[19], S. Mitra[60], V. P. Mitrofanov[30], G. Mitselmakher[15], R. Mittleman[24], B. Moe[13], M. Mohan[22], S. R. P. Mohapatra[23,48], F. Mokler[10,9], D. Moraru[18], G. Moreno[18], N. Morgado[35], T. Mori[66], S. R. Morriss[44], K. Mossavi[9,10], B. Mours[4], C. M. Mow–Lowry[9,10], C. L. Mueller[15], G. Mueller[15], S. Mukherjee[44], A. Mullavey[2,54], J. Munch[87], D. Murphy[26], P. G. Murray[3], A. Mytidis[15], D. Nanda Kumar[15], T. Nash[1], L. Naticchioni[17ab], R. Nayak[88], V. Necula[15], I. Neri[37ab], G. Newton[3], T. Nguyen[54], E. Nishida[66], A. Nishizawa[66], A. Nitz[23], F. Nocera[22], D. Nolting[6], M. E. Normandin[44], L. Nuttall[7], E. Ochsner[13], J. O'Dell[68], E. Oelker[24], G. H. Ogin[1], J. J. Oh[89], S. H. Oh[89], F. Ohme[7], P. Oppermann[9,10], B. O'Reilly[6], R. O'Shaughnessy[13], C. Osthelder[1], C. D. Ott[51], D. J. Ottaway[87], R. S. Ottens[15], J. Ou[101], H. Overmier[6], B. J. Owen[64], C. Padilla[70], A. Page[19], A. Pai[72], L. Palladino[49ac], C. Palomba[17a], Y. Pan[41], C. Pankow[13], F. Paoletti[14a,22], R. Paoletti[14ac], M. A. Papa[20,13], H. Paris[18], M. Parisi[5ab], W. Parkinson[90], A. Pasqualetti[22], R. Passaquieti[14ab], D. Passuello[14a], M. Pedraza[1], S. Penn[79], C. Peralta[20], A. Perreca[23], M. Phelps[1], M. Pichot[34a], M. Pickenpack[9,10], F. Piergiovanni[38ab], V. Pierro[8], L. Pinard[35], I. M. Pinto[8], M. Pitkin[3], H. J. Pletsch[9,10], R. Poggiani[14ab], J. Pöld[9,10], F. Postiglione[91], C. Poux[1], V. Predoi[7], T. Prestegard[78], L. R. Price[1], M. Prijatelj[9,10], S. Privitera[1], G. A. Prodi[61ab], L. G. Prokhorov[30], O. Puncken[44], M. Punturo[37a], P. Puppo[17a], V. Quetschke[44], E. Quintero[1], R. Quitzow-James[39], F. J. Raab[18], D. S. Rabeling[11ab], I. Rácz[59], H. Radkins[18], P. Raffai[26], S. Raja[92], M. Rakhmanov[44], C. Ramet[6], P. Rapagnani[17ab], V. Raymond[1], V. Re[49ab], C. M. Reed[18], T. Reed[93], T. Regimbau[34a], S. Reid[94], D. H. Reitze[1], F. Ricci[17ab], R. Riesen[6], K. Riles[47], M. Roberts[27], N. A. Robertson[1,3], F. Robinet[31a], E. L. Robinson[20], A. Rocchi[49a], S. Roddy[6], C. Rodriguez[63], L. Rodriguez[85], M. Rodruck[18], L. Rolland[4], J. G. Rollins[1], J. D. Romano[44], R. Romano[5ac], J. H. Romie[6],

D. Rosińska[28cf], C. Röver[9,10], S. Rowan[3], A. Rüdiger[9,10], P. Ruggi[22], K. Ryan[18], F. Salemi[9,10], L. Sammut[56], V. Sandberg[18], J. Sanders[47], S. Sankar[24], V. Sannibale[1], L. Santamaría[1], I. Santiago-Prieto[3], E. Saracco[35], B. Sassolas[35], B. S. Sathyaprakash[7], P. R. Saulson[23], R. L. Savage[18], R. Schilling[9,10], R. Schnabel[9,10], R. M. S. Schofield[39], D. Schuette[9,10], B. Schulz[9,10], B. F. Schutz[20,7], P. Schwinberg[18], J. Scott[3], S. M. Scott[54], F. Seifert[1], D. Sellers[6], A. S. Sengupta[95], D. Sentenac[22], A. Sergeev[80], D. A. Shaddock[54], S. Shah[96], M. Shaltev[9,10], Z. Shao[1], B. Shapiro[27], P. Shawhan[41], D. H. Shoemaker[24], T. L Sidery[19], X. Siemens[13], D. Sigg[18], D. Simakov[9,10], A. Singer[1], L. Singer[1], A. M. Sintes[42], G. R. Skelton[13], B. J. J. Slagmolen[54], J. Slutsky[9,10], J. R. Smith[70], M. R. Smith[1], R. J. E. Smith[19], N. D. Smith-Lefebvre[1], E. J. Son[89], B. Sorazu[3], T. Souradeep[60], L. Sperandio[49ab], M. Stefszky[54], E. Steinert[18], J. Steinlechner[9,10], S. Steinlechner[9,10], S. Steplewski[36], D. Stevens[63], A. Stochino[54], R. Stone[44], K. A. Strain[3], S. E. Strigin[30], A. S. Stroeer[44], R. Sturani[38ab], A. L. Stuver[6], T. Z. Summerscales[97], S. Susmithan[33], P. J. Sutton[7], B. Swinkels[22], G. Szeifert[65], M. Tacca[22], L. Taffarello[61c], D. Talukder[39], D. B. Tanner[15], S. P. Tarabrin[9,10], R. Taylor[1], A. P. M. ter Braack[11a], M. Thomas[6], P. Thomas[18], K. A. Thorne[6], K. S. Thorne[51], E. Thrane[1], V. Tiwari[15], K. V. Tokmakov[84], C. Tomlinson[58], A. Toncelli[14ab], M. Tonelli[14ab], O. Torre[14ac], C. V. Torres[44], C. I. Torrie[1,3], E. Tournefier[4], F. Travasso[37ab], G. Traylor[6], M. Tse[26], D. Ugolini[98], C. S. Unnikrishnan[99], H. Vahlbruch[10,9], G. Vajente[14ab], M. Vallisneri[51], J. F. J. van den Brand[11ab], C. Van Den Broeck[11a], S. van der Putten[11a], M. V. van der Sluys[63], A. A. van Veggel[3], S. Vass[1], M. Vasuth[59], R. Vaulin[24], M. Vavoulidis[31a], A. Vecchio[19], G. Vedovato[61c], J. Veitch[7], K. Venkateswara[100], D. Verkindt[4], S. Verma[33], F. Vetrano[38ab], A. Viceré[38ab], R. Vincent-Finley[86], J.-Y. Vinet[34a], S. Vitale[24], S. Vitale[11a], T. Vo[18], H. Vocca[37a], C. Vorvick[18], W. D. Vousden[19], S. P. Vyatchanin[30], A. Wade[54], L. Wade[13], M. Wade[13], S. J. Waldman[24], L. Wallace[1], Y. Wan[46], J. Wang[101], M. Wang[19], X. Wang[46], A. Wanner[9,10], R. L. Ward[25,54], M. Was[9,10,31a], M. Weinert[9,10], A. J. Weinstein[1], R. Weiss[24], T. Welborn[6], L. Wen[33], P. Wessels[9,10], M. West[23], T. Westphal[9,10], K. Wette[9,10], J. T. Whelan[48], D. J. White[58], B. F. Whiting[15], K. Wiesner[9,10], C. Wilkinson[18], P. A. Willems[1], L. Williams[15], R. Williams[1], T. Williams[90], J. L. Willis[102], B. Willke[9,10], M. Wimmer[9,10], L. Winkelmann[9,10], W. Winkler[9,10], C. C. Wipf[24], A. G. Wiseman[13], H. Wittel[9,10], G. Woan[3], R. Wooley[6], J. Worden[18], J. Yablon[63], I. Yakushin[6], H. Yamamoto[1], C. C. Yancey[41], H. Yang[51], D. Yeaton-Massey[1], S. Yoshida[90], H. Yum[63], M. Yvert[4], A. Zadrożny[28e], M. Zanolin[69], J.-P. Zendri[61c], F. Zhang[24], L. Zhang[1], C. Zhao[33], H. Zhu[64], X. J. Zhu[33], N. Zotov[93], M. E. Zucker[24], J. Zweizig[1]

(The LIGO Scientific Collaboration and the Virgo Collaboration)

[1] *LIGO - California Institute of Technology, Pasadena, CA 91125, USA*

[2] *Louisiana State University, Baton Rouge, LA 70803, USA*

[3] *SUPA, University of Glasgow, Glasgow, G12 8QQ, United Kingdom*

[4] *Laboratoire d'Annecy-le-Vieux de Physique des Particules (LAPP), Université de Savoie, CNRS/IN2P3, F-74941 Annecy-Le-Vieux, France*

[5] *INFN, Sezione di Napoli [a]; Università di Napoli 'Federico II'[b], Complesso Universitario di Monte S.Angelo, I-80126 Napoli; Università di Salerno, Fisciano, I-84084 Salerno[c], Italy*

[6] *LIGO - Livingston Observatory, Livingston, LA 70754, USA*

[7] *Cardiff University, Cardiff, CF24 3AA, United Kingdom*

[8] *University of Sannio at Benevento, I-82100 Benevento, Italy and INFN (Sezione di Napoli), Italy*

[9] *Albert-Einstein-Institut, Max-Planck-Institut für Gravitationsphysik, D-30167 Hannover, Germany*

[10] *Leibniz Universität Hannover, D-30167 Hannover, Germany*

[11] *Nikhef, Science Park, Amsterdam, The Netherlands[a]; VU University Amsterdam, De Boelelaan 1081, 1081 HV Amsterdam, The Netherlands[b]*

[12] *Instituto Nacional de Pesquisas Espaciais, 12227-010 - São José dos Campos, SP, Brazil*

[13] *University of Wisconsin–Milwaukee, Milwaukee, WI 53201, USA*

[14] *INFN, Sezione di Pisa[a]; Università di Pisa[b]; I-56127 Pisa; Università di Siena, I-53100 Siena[c], Italy*

[15] *University of Florida, Gainesville, FL 32611, USA*

[16] *The University of Mississippi, University, MS 38677, USA*

[17] *INFN, Sezione di Roma[a]; Università 'La Sapienza'[b], I-00185 Roma, Italy*

[18] *LIGO - Hanford Observatory, Richland, WA 99352, USA*
[19] *University of Birmingham, Birmingham, B15 2TT, United Kingdom*
[20] *Albert-Einstein-Institut, Max-Planck-Institut für Gravitationsphysik, D-14476 Golm, Germany*
[21] *Montana State University, Bozeman, MT 59717, USA*
[22] *European Gravitational Observatory (EGO), I-56021 Cascina (PI), Italy*
[23] *Syracuse University, Syracuse, NY 13244, USA*
[24] *LIGO - Massachusetts Institute of Technology, Cambridge, MA 02139, USA*
[25] *APC, AstroParticule et Cosmologie, Université Paris Diderot, CNRS/IN2P3, CEA/Irfu, Observatoire de Paris, Sorbonne Paris Cité, 10, rue Alice Domon et Léonie Duquet, F-75205 Paris Cedex 13, France*
[26] *Columbia University, New York, NY 10027, USA*
[27] *Stanford University, Stanford, CA 94305, USA*
[28] *IM-PAN 00-956 Warsaw[a]; Astronomical Observatory Warsaw University 00-478 Warsaw[b]; CAMK-PAN 00-716 Warsaw[c]; Białystok University 15-424 Białystok[d]; NCBJ 05-400 Świerk-Otwock[e]; Institute of Astronomy 65-265 Zielona Góra[f], Poland*
[29] *San Jose State University, San Jose, CA 95192, USA*
[30] *Moscow State University, Moscow, 119992, Russia*
[31] *LAL, Université Paris-Sud, IN2P3/CNRS, F-91898 Orsay[a]; ESPCI, CNRS, F-75005 Paris[b], France*
[32] *NASA/Goddard Space Flight Center, Greenbelt, MD 20771, USA*
[33] *University of Western Australia, Crawley, WA 6009, Australia*
[34] *Université Nice-Sophia-Antipolis, CNRS, Observatoire de la Côte d'Azur, F-06304 Nice[a]; Institut de Physique de Rennes, CNRS, Université de Rennes 1, F-35042 Rennes[b], France*
[35] *Laboratoire des Matériaux Avancés (LMA), IN2P3/CNRS, Université de Lyon, F-69622 Villeurbanne, Lyon, France*
[36] *Washington State University, Pullman, WA 99164, USA*
[37] *INFN, Sezione di Perugia[a]; Università di Perugia[b], I-06123 Perugia; Universita' di Camerino, Dipartimento di Fisica[c], I-62032 Camerino, Italy*
[38] *INFN, Sezione di Firenze, I-50019 Sesto Fiorentino[a]; Università degli Studi di Urbino 'Carlo Bo', I-61029 Urbino[b], Italy*
[39] *University of Oregon, Eugene, OR 97403, USA*
[40] *Laboratoire Kastler Brossel, ENS, CNRS, UPMC, Université Pierre et Marie Curie, 4 Place Jussieu, F-75005 Paris, France*
[41] *University of Maryland, College Park, MD 20742 USA*
[42] *Universitat de les Illes Balears, E-07122 Palma de Mallorca, Spain*
[43] *University of Massachusetts - Amherst, Amherst, MA 01003, USA*
[44] *The University of Texas at Brownsville, Brownsville, TX 78520, USA*
[45] *Canadian Institute for Theoretical Astrophysics, University of Toronto, Toronto, Ontario, M5S 3H8, Canada*
[46] *Tsinghua University, Beijing 100084 China*
[47] *University of Michigan, Ann Arbor, MI 48109, USA*
[48] *Rochester Institute of Technology, Rochester, NY 14623, USA*
[49] *INFN, Sezione di Roma Tor Vergata[a]; Università di Roma Tor Vergata, I-00133 Roma[b]; Università dell'Aquila, I-67100 L'Aquila[c], Italy*
[50] *Charles Sturt University, Wagga Wagga, NSW 2678, Australia*
[51] *Caltech-CaRT, Pasadena, CA 91125, USA*
[52] *INFN, Sezione di Genova; I-16146 Genova, Italy*
[53] *Pusan National University, Busan 609-735, Korea*
[54] *Australian National University, Canberra, ACT 0200, Australia*
[55] *Carleton College, Northfield, MN 55057, USA*

[56] *The University of Melbourne, Parkville, VIC 3010, Australia*
[57] *University of Cambridge, Cambridge, CB2 1TN, United Kingdom*
[58] *The University of Sheffield, Sheffield S10 2TN, United Kingdom*
[59] *Wigner RCP, RMKI, H-1121 Budapest, Konkoly Thege Miklós út 29-33, Hungary*
[60] *Inter-University Centre for Astronomy and Astrophysics, Pune - 411007, India*
[61] *INFN, Gruppo Collegato di Trento[a] and Università di Trento[b], I-38050 Povo, Trento, Italy; INFN, Sezione di Padova[c] and Università di Padova[d], I-35131 Padova, Italy*
[62] *California Institute of Technology, Pasadena, CA 91125, USA*
[63] *Northwestern University, Evanston, IL 60208, USA*
[64] *The Pennsylvania State University, University Park, PA 16802, USA*
[65] *Eötvös Loránd University, Budapest, 1117 Hungary*
[66] *National Astronomical Observatory of Japan, Tokyo 181-8588, Japan*
[67] *University of Szeged, 6720 Szeged, Dóm tér 9, Hungary*
[68] *Rutherford Appleton Laboratory, HSIC, Chilton, Didcot, Oxon OX11 0QX United Kingdom*
[69] *Embry-Riddle Aeronautical University, Prescott, AZ 86301 USA*
[70] *California State University Fullerton, Fullerton CA 92831 USA*
[71] *Perimeter Institute for Theoretical Physics, Ontario, N2L 2Y5, Canada*
[72] *IISER-TVM, CET Campus, Trivandrum Kerala 695016, India*
[73] *American University, Washington, DC 20016, USA*
[74] *University of New Hampshire, Durham, NH 03824, USA*
[75] *Raman Research Institute, Bangalore, Karnataka 560080, India*
[76] *Korea Institute of Science and Technology Information, Daejeon 305-806, Korea*
[77] *University of Southampton, Southampton, SO17 1BJ, United Kingdom*
[78] *University of Minnesota, Minneapolis, MN 55455, USA*
[79] *Hobart and William Smith Colleges, Geneva, NY 14456, USA*
[80] *Institute of Applied Physics, Nizhny Novgorod, 603950, Russia*
[81] *Hanyang University, Seoul 133-791, Korea*
[82] *Universidad Nacional de Cordoba, Cordoba 5000, Argentina*
[83] *Seoul National University, Seoul 151-742, Korea*
[84] *University of Strathclyde, Glasgow, G1 1XQ, United Kingdom*
[85] *The University of Texas at Austin, Austin, TX 78712, USA*
[86] *Southern University and A&M College, Baton Rouge, LA 70813, USA*
[87] *University of Adelaide, Adelaide, SA 5005, Australia*
[88] *IISER-Kolkata, Mohanpur West. Bengal 741252, India*
[89] *National Institute for Mathematical Sciences, Daejeon 305-390, Korea*
[90] *Southeastern Louisiana University, Hammond, LA 70402, USA*
[91] *University of Salerno, I-84084 Fisciano (Salerno), Italy*
[92] *RRCAT, Indore MP 452013, India*
[93] *Louisiana Tech University, Ruston, LA 71272, USA*
[94] *SUPA, University of the West of Scotland, Paisley, PA1 2BE, United Kingdom*
[95] *Indian Institute of Technology, Gandhinagar Ahmedabad Gujarat 382424, India*
[96] *Department of Astrophysics/IMAPP, Radboud University Nijmegen, P.O. Box 9010, 6500 GL Nijmegen, The Netherlands; Nikhef, Science Park, Amsterdam, The Netherlands*
[97] *Andrews University, Berrien Springs, MI 49104 USA*
[98] *Trinity University, San Antonio, TX 78212, USA*
[99] *Tata Institute for Fundamental Research, Mumbai 400005, India*
[100] *University of Washington, Seattle, WA, 98195-4290, USA*

[101] *National Tsing Hua University, Hsinchu Taiwan 300, Province of China*
[102] *Abilene Christian University, Abilene TX 79699, USA*
[103] *The George Washington University, Washington, DC 20052, USA*

April 24, 2014

Abstract

We present a possible observing scenario for the Advanced LIGO and Advanced Virgo gravitational wave detectors over the next decade, with the intention of providing information to the astronomy community to facilitate planning for multi-messenger astronomy with gravitational waves. We determine the expected sensitivity of the network to transient gravitational-wave signals, and study the capability of the network to determine the sky location of the source. For concreteness, we focus primarily on gravitational-wave signals from the inspiral of binary neutron star (BNS) systems, as the source considered likely to be the most common for detection and also promising for multimessenger astronomy. We find that confident detections will likely require at least 2 detectors operating with BNS sensitive ranges of at least 100 Mpc, while ranges approaching 200 Mpc should give at least $\sim$1 BNS detection per year even under pessimistic predictions of signal rates. The ability to localize the source of the detected signals depends on the geographical distribution of the detectors and their relative sensitivity, and can be as large as thousands of square degrees with only 2 sensitive detectors operating. Determining the sky position of a significant fraction of detected signals to areas of $5\,\mathrm{deg}^2$ to $20\,\mathrm{deg}^2$ will require at least 3 detectors of sensitivity within a factor of ~ 2 of each other and with a broad frequency bandwidth. Should one of the LIGO detectors be relocated in India as expected, many gravitational-wave signals will be localized to a few square degrees by gravitational-wave observations alone.

1 Introduction

Advanced LIGO (aLIGO) [1] and Advanced Virgo (AdV) [2, 3] are kilometer-scale gravitational wave (GW) detectors that are expected to yield direct observations of gravitational waves. In this document we describe the currently projected schedule, sensitivity, and sky localization accuracy for the GW detector network. The purpose of this document is to provide information to the astronomy community to assist in the formulation of plans for the upcoming era of GW observations. In particular, we intend this document to provide the information required for assessing the features of programs for joint observation of GW events using electromagnetic, neutrino, or other observing facilities.

The full science of aLIGO and AdV is broad [4], and is not covered in this document. We concentrate solely on candidate GW transient signals. We place particular emphasis on the coalescence of neutron-star binary systems, which are the GW source with the most reliable predictions on the prospects of detection.

Although our collaborations have amassed a great deal of experience with GW detectors and analysis, it is still very difficult to make predictions for both improvements in search methods and for the rate of progress for detectors which are not yet fully installed or operational. *We stress that the scenarios of LIGO and Virgo detector sensitivity evolution and observing times given here represent our best estimates at present. They should not be considered as fixed or firm commitments.* As the detectors' construction and commissioning progresses, we intend to release updates versions of this document.

2 Commissioning and Observing Phases

We divide the roadmap for the aLIGO and AdV observatories into three phases:

1. **Construction** includes the installation and testing of the detectors. This phase ends with *acceptance* of the detectors. Acceptance means that the interferometers can lock for periods of hours: light is resonant in the arms of the interferometer with *no guaranteed gravitational-wave sensitivity.* Construction will likely involve several short *engineering runs* with no expected astrophysical output as the detectors progress towards acceptance.

2. **Commissioning** will take the detectors from their configuration at acceptance through progressively better sensitivity to the ultimate second-generation detector sensitivity. Engineering and *science* runs in the commissioning phase will allow us to understand our detectors and analyses in an observational mode. It is expected that science runs will produce astrophysical results, including upper limits on the rate of sources and quite possibly the first detections of GWs. During this phase, exchange of GW candidates with partners outside the LSC and Virgo collaborations will be governed by memoranda of understanding (MOUs) [5].

3. **Observing** runs begin when the detectors are at a sensitivity which makes detections likely. We anticipate that there will be a gradual transition from the commissioning to the observing phases. If it has not happened previously, the first few GW signals will be observed and the LSC and Virgo will be engaged in a long-term campaign to observe the GW sky. After the first four detections [5] we expect free exchange of GW event candidates with the astronomical community and the maturation of GW astronomy.

The progress in sensitivity as a function of time will affect the duration of the runs that we plan at any stage, as we strive to minimize the time to the first gravitational wave detection. Commissioning is a complex process which involves both scheduled improvements to the detectors and tackling unexpected new problems. While our experience makes us cautiously optimistic regarding the schedule for the advanced detectors, we note that we are targeting an order of magnitude improvement in sensitivity relative to the previous generation of detectors over a much wider frequency band. Consequently it is not possible to make concrete predictions for sensitivity as a function of time. We can, however, use our previous experience as a guide to plausible scenarios for the detector operational states that will allow us to reach the desired sensitivity. Unexpected problems could slow down the commissioning, but there is also the possibility that progress may happen faster than predicted here. As the detectors begin to be commissioned, information on the cost in time and benefit in sensitivity will become more apparent and drive the schedule of runs. More information on event rates, including the first detection, will also very likely change the schedule and duration of runs. In section 2.1 we present the commissioning plans for the aLIGO and AdV detectors. A summary of expected science runs is in section 2.2.

2.1 Commissioning and Observing Roadmap

The anticipated strain sensitivity evolution for aLIGO and AdV is shown in Fig. 1. A standard figure of merit for the sensitivity of an interferometer is the binary neutron star (BNS) *range*: the volume- and orientation-averaged distance at which a compact binary coalescence consisting of two $1.4\,\mathrm{M}_\odot$ neutron stars gives a matched filter signal-to-noise ratio of 8 in a single detector [6][1]. The

[1] Another often quoted number is the BNS *horizon*—the distance at which an optimally oriented and located BNS system would be observed with a signal to noise ratio of 8. The horizon is a factor of 2.26 larger than the range.

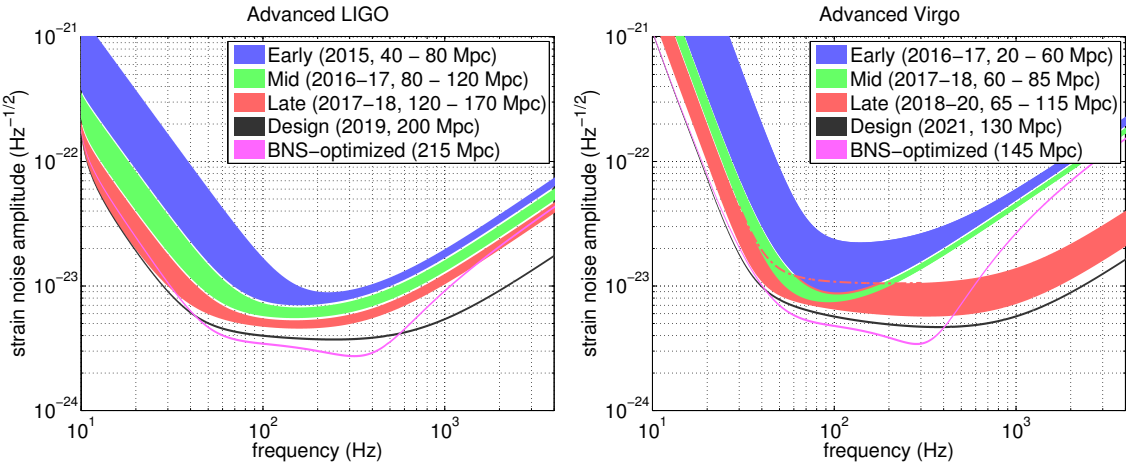

Figure 1: aLIGO (left) and AdV (right) target strain sensitivity as a function of frequency. The average distance to which binary neutron star (BNS) signals could be seen is given in Mpc. Current notions of the progression of sensitivity are given for early, middle, and late commissioning phases, as well as the final design sensitivity target and the BNS-optimized sensitivity. While both dates and sensitivity curves are subject to change, the overall progression represents our best current estimates.

BNS ranges for the various stages of aLIGO and AdV expected evolution are also provided in Fig. 1.

The installation of aLIGO is well underway. The plan calls for three identical 4 km interferometers, referred to as H1, H2, and L1. In 2011, the LIGO Lab and IndIGO consortium in India proposed installing one of the aLIGO Hanford detectors, H2, at a new observatory in India (LIGO-India). As of early 2013 LIGO Laboratory has begun preparing the H2 interferometer for shipment to India. Funding for the Indian portion of LIGO-India is in the final stages of consideration by the Indian government.

The first aLIGO science run is expected in 2015. It will be of order three months in duration, and will involve the H1 and L1 detectors (assuming H2 is placed in storage for LIGO-India). The detectors will *not* be at full design sensitivity; we anticipate a possible BNS range of 40 – 80 Mpc. Subsequent science runs will have increasing duration and sensitivity. We aim for a BNS range of 80 – 170 Mpc over 2016–18, with science runs of several months. Assuming that no unexpected obstacles are encountered, the aLIGO detectors are expected to achieve a 200 Mpc BNS range circa 2019. After the first observing runs, circa 2020, it might be desirable to optimize the detector sensitivity for a specific class of astrophysical signals, such as BNSs. The BNS range may then become 215 Mpc. The sensitivity for each of these stages is shown in Fig. 1.

Because of the planning for the installation of one of the LIGO detectors in India, the installation of the H2 detector has been deferred. This detector will be reconfigured to be identical to H1 and L1 and will be installed in India once the LIGO-India Observatory is complete. The final schedule will be adopted once final funding approvals are granted. It is expected that the site development would start in 2014, with installation of the detector beginning in 2018. Assuming no unexpected problems, first runs are anticipated circa 2020 and design sensitivity at the same level as the H1 and L1 detectors is anticipated for no earlier than 2022.

The commissioning timeline for AdV [3] is still being defined, but it is anticipated that in

2015 AdV might join the LIGO detectors in their first science run depending on the sensitivity attained. Following an early step with sensitivity corresponding to a BNS range of 20 – 60 Mpc, commissioning is expected to bring AdV to a 60 – 85 Mpc in 2017–18. A configuration upgrade at this point will allow the range to increase to approximately 65 – 115 Mpc in 2018–20. The final design sensitivity, with a BNS range of 130 Mpc, is anticipated circa 2021. The corresponding BNS-optimised range would be 145 Mpc. The sensitivity curves for the various AdV configurations are shown in Fig. 1.

The GEO600 [7] detector will likely be operational in the early to middle phase of the AdV and aLIGO science runs, i.e. from 2015–2017. The sensitivity that potentially can be achieved by GEO in this timeframe is similar to the AdV sensitivity of the early and mid scenarios at frequencies around 1 kHz and above. Around 100 Hz GEO will be at least 10 times less sensitive than the early AdV and aLIGO detectors.

Japan has recently begun the construction of an advanced detector, KAGRA [8]. KAGRA is designed to have a BNS range comparable to AdV at final sensitivity. While we do not consider KAGRA in this document, we note that the addition of KAGRA to the worldwide GW detector network will improve both sky coverage and localization capabilities beyond those envisioned here.

2.2 Estimated observing schedule

Keeping in mind the mentioned important caveats about commissioning affecting the scheduling and length of science runs, the following is a plausible scenario for the operation of the LIGO-Virgo network over the next decade:

- 2015: A 3 month run with the two-detector H1L1 network at early aLIGO sensitivity (40 – 80 Mpc BNS range). Virgo in commissioning at $\sim$ 20 Mpc with a chance to join the run.
- 2016–17: A 6 month run with H1L1 at 80 – 120 Mpc and Virgo at 20 – 60 Mpc.
- 2017–18: A 9 month run with H1L1 at 120 – 170 Mpc and Virgo at 60 – 85 Mpc.
- 2019+: Three-detector network with H1L1 at full sensitivity of 200 Mpc and V1 at 65 – 130 Mpc.
- 2022+: Four-detector H1L1V1+LIGO-India network at full sensitivity (aLIGO at 200 Mpc, AdV at 130 Mpc).

The observational implications of this scenario are discussed in section 4.

3 Searches for gravitational-wave transients

Data from gravitational wave detectors are searched for many types of possible signals [4]. Here we focus on signals from compact binary coalescences (CBC), including BNS systems, and on generic transient or *burst* signals. See [9, 10, 11] for recent observational results from LIGO and Virgo for such systems.

The gravitational waveform from a binary neutron star coalescence is well modelled and matched filtering can be used to search for signals and measure the system parameters. For systems containing black holes, or in which the component spin is significant, uncertainties in the waveform model can reduce the sensitivity of the search. Searches for bursts make few assumptions on the signal morphology, using time-frequency decompositions to identify statistically significant excess power transients in the data. Burst searches generally perform best for short-duration signals

($\lesssim$1 s); their astrophysical targets include core-collapse supernovae, magnetar flares, black hole binary coalescence, cosmic string cusps, and possibly as-yet-unknown systems.

In the era of advanced detectors, the LSC and Virgo will search in *near real-time* for CBC and burst signals for the purpose of rapidly identifying event candidates. A prompt notice of a potential GW transient by LIGO-Virgo might enable followup observations in the electromagnetic spectrum. A first followup program including low-latency analysis, event candidate selection, position reconstruction and the sending of alerts to several observing partners (optical, X-ray, and radio) was implemented and exercised during the 2009–2010 LIGO-Virgo science run [12, 13, 14]. Latencies of less than 1 hour were achieved and we expect to improve this in the advanced detector era. Increased detection confidence, improved sky localization, and identification of host galaxy and redshift are just some of the benefits of joint GW-electromagnetic observations. With this in mind, we focus on two points of particular relevance for followup of GW events: the source localization afforded by a GW network and the relationship between signal significance (or false alarm rate) and localization.

3.1 Localization

The aLIGO-AdV network will determine the sky position of a GW transient source mainly by triangulation using the observed time delays between sites [15, 16]. The effective single-site timing accuracy is approximately

$$\sigma_t = \frac{1}{2\pi\rho\sigma_f}\,, \tag{1}$$

where ρ is the signal-to-noise ratio in the given detector and σ_f is the effective bandwidth of the signal in the detector, typically of order 100 Hz. Thus a typical timing accuracy is on the order of 10^{-4} s (about 1/100 of the light travel time between sites). This sets the localization scale. Equation (1) ignores many other relevant issues such as uncertainty in the emitted gravitational waveform, instrumental calibration accuracies, and correlation of sky location with other binary parameters [15, 17, 18, 19, 20, 21]. While many of these will affect the measurement of the time of arrival in individual detectors, such factors are largely common between two similar detectors, so the time difference between the two detectors is relatively uncorrelated with these "nuisance" parameters. The triangulation approach therefore provides a good leading order estimate to localizations.

Source localization using only timing for a 2-site network yields an annulus on the sky; see Fig. 2. Additional information such as signal amplitude, spin, and precessional effects can sometimes resolve this to only parts of the annulus, but even then sources will only be localized to regions of hundreds to thousands of square degrees. For three detectors, the time delays restrict the source to two sky regions whose locations are mirror images in the plane formed by the three detectors. It is often possible to eliminate one of these regions by requiring consistent amplitudes in all detectors. For signals just above the detection threshold, this typically yields regions with areas of several tens of square degrees. If there is significant difference in sensitivity between detectors, the source is less well localized and we may be left with the majority of the annulus on the sky determined by the two most sensitive detectors. With four or more detectors, timing information alone is sufficient to localize to a single sky region, and the additional baselines help to limit the region to under 10 square degrees for some signals.

From (1), it follows that the *linear* size of the localization ellipse scales inversely with the signal to noise ratio (SNR) of the signal and the frequency bandwidth of the signal in the detector. For GWs that sweep across the band of the detector, such as binary merger signals, the effective

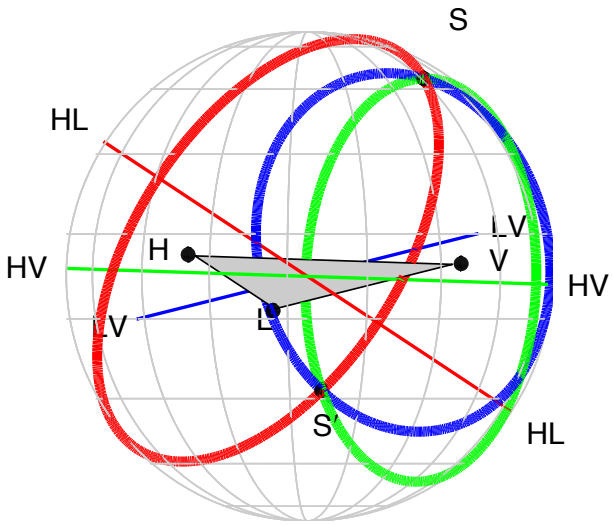

Figure 2: Source localization by triangulation for the aLIGO-AdV network. The locus of constant time delay (with associated timing uncertainty) between two detectors forms an annulus on the sky concentric about the baseline between the two sites. For three detectors, these annuli may intersect in two locations. One is centered on the true source direction, S, while the other (S') is its mirror image with respect to the geometrical plane passing through the three sites. For four or more detectors there is a unique intersection region of all of the annuli. Figure adapted from [22].

bandwidth is $\sim 100\,\mathrm{Hz}$, determined by the most sensitive frequencies of the detector. For shorter transients the bandwidth σ_f depends on the specific signal. For example, GWs emitted by various processes in core-collapse supernovae are anticipated to have relatively large bandwidths, between 150-500 Hz [23, 24, 25, 26], largely independent of detector configuration. By contrast, the sky localization region for narrowband burst signals may consist of multiple disconnected regions; see for example [27, 12].

Finally, we note that some GW searches are triggered by electromagnetic observations, and in these cases localization information is known *a priori*. For example, in GW searches triggered by gamma-ray bursts [10] the triggering satellite provides the localization. The rapid identification of a GW counterpart to such a trigger could prompt further followups by other observatories. This is of particular relevance to binary mergers, which are considered the likely progenitors of most short gamma-ray bursts. It is therefore important to have high-energy satellites operating during the advanced detector era.

Finally, it is also worth noting that all GW data are stored permanently, so that it is possible to perform retroactive analyses at any time.

3.2 Detection and False Alarm Rates

The rate of BNS coalescences is uncertain, but is currently predicted to lie between $10^{-8} - 10^{-5}\,\mathrm{Mpc}^{-3}\,\mathrm{yr}^{-1}$ [28]. This corresponds to between 0.4 and 400 signals above SNR 8 per year of observation for a single aLIGO detector at final sensitivity [28]. The predicted observable rates for NS-BH and BBH are similar. Expected rates for other transient sources are lower and/or less well constrained.

The rate of false alarm triggers above a given SNR will depend critically upon the data quality of

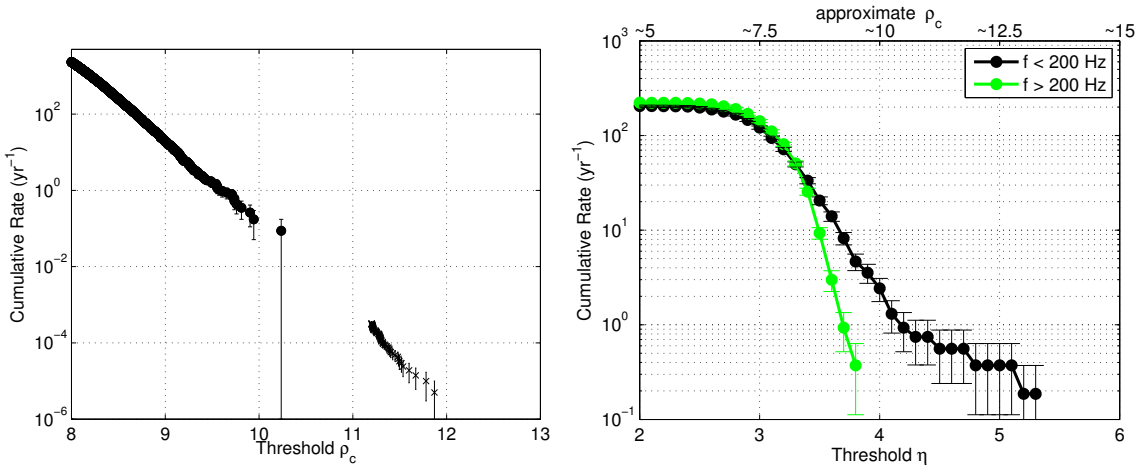

Figure 3: False alarm rate versus detection statistic for CBC and burst searches on 2009-2010 LIGO-Virgo data. Left: Cumulative rate of background events for the CBC search, as a function of the threshold ranking statistic ρ_c [9]. Right: Cumulative rate of background events for the burst search, as a function of the coherent network amplitude η [11]. In the large-amplitude limit η is related to the combined SNR by $\rho_c \sim \sqrt{2K}\eta$, where K is the number of detectors. The burst events are divided into two sets based on their central frequency.

the advanced detectors; non-stationary transients or *glitches* will produce an elevated background of loud triggers. For low-mass binary coalescence searches, the waveforms are well modelled and signal consistency tests reduce the background significantly. For burst sources which are not well modelled, or which spend only a short time in the detectors' sensitive band, it is more difficult to distinguish between the signal and a glitch, and so a reduction of the false alarm rate comes at a higher cost in terms of reduced detection efficiency.

Figure 3 shows the noise background as a function of detection statistic for the low-mass binary coalescence and burst searches with the 2009–2010 LIGO-Virgo data [9, 11]. For binary mergers, the background rate decreases by a factor of ∼100 for every unit increase in combined SNR ρ_c, with no evidence of a tail even at low false alarm rates. Here, ρ_c is a combined, re-weighted SNR. The re-weighting is designed to reduce the SNR of glitches while leaving signals largely unaffected. Consequently, for a signal ρ_c is essentially the root-sum-square of the SNRs in the individual detectors.

We conservatively estimate a ρ_c threshold of 12 is required for a false rate below $\sim 10^{-2}\,\mathrm{yr}^{-1}$ in aLIGO-AdV, where we have taken into account trials factors due to the increase in the number of template waveforms required to search the advanced detector data. In future sections, we quote results for this threshold. A combined SNR of 12 corresponds to a single detector SNR of 8.5 in each of two detectors or 7 in three detectors. At this threshold we estimate approximately a quarter of detected signals can be localized with 90% containment to areas of $20\,\mathrm{deg}^2$ or less by the H1L1V1 network at design sensitivity; see the 2019+ epoch in Table 1 for details. For a background rate of $1\,\mathrm{yr}^{-1}$ ($100\,\mathrm{yr}^{-1}$) the threshold ρ_c decreases by about 10% (20%), the number of signals above threshold increases by about 30% (90%), and the area localization for these low-threshold signals is degraded by approximately 20% (60%).

Imperfections in the data can have a greater effect on the burst search. At frequencies above

200 Hz the rate of background events falls off steeply as a function of amplitude. At lower frequencies, however, the data often exhibit a significant tail of loud background events that are not removed by multi-detector consistency tests. While the extent of these tails varies, when present they typically begin at rates of approximately $1\,\mathrm{yr}^{-1}$, hindering the confident detection of low-frequency gravitational-wave transients. Although the advanced detectors are designed with many technical improvements, we must anticipate that burst searches will likely still have to deal with such tails in some cases, particularly at low frequencies. The unambiguous observation of an electromagnetic counterpart could increase the detection confidence in these cases.

A study [27] of the localization capability of the burst search for the aLIGO-AdV network using a variety of waveform morphologies finds that at an SNR of $\rho_c \simeq 17$ (false rate of $\lesssim 0.1\,\mathrm{yr}^{-1}$ from Fig. 3) the typical error box area for 50% (90%) containment is approximately $40\,\mathrm{deg}^2$ ($400\,\mathrm{deg}^2$). The median 50% containment area increases to $100\,\mathrm{deg}^2$ at $\rho_c \simeq 12$, and drops to approximately $16\,\mathrm{deg}^2$ at $\rho_c \simeq 25$. These results are broadly consistent with a study of two burst detection algorithms using real LIGO-Virgo data from 2009 [12], which shows that for signals near the nominal search threshold (coherent network amplitude $\eta \gtrsim 6$, corresponding $\rho_c \gtrsim 15$ [11]) median containment regions are typically between $30\,\mathrm{deg}^2$ and $200\,\mathrm{deg}^2$, dropping to approximately $10\,\mathrm{deg}^2$ at large amplitudes. See Fig. 4 for an example.

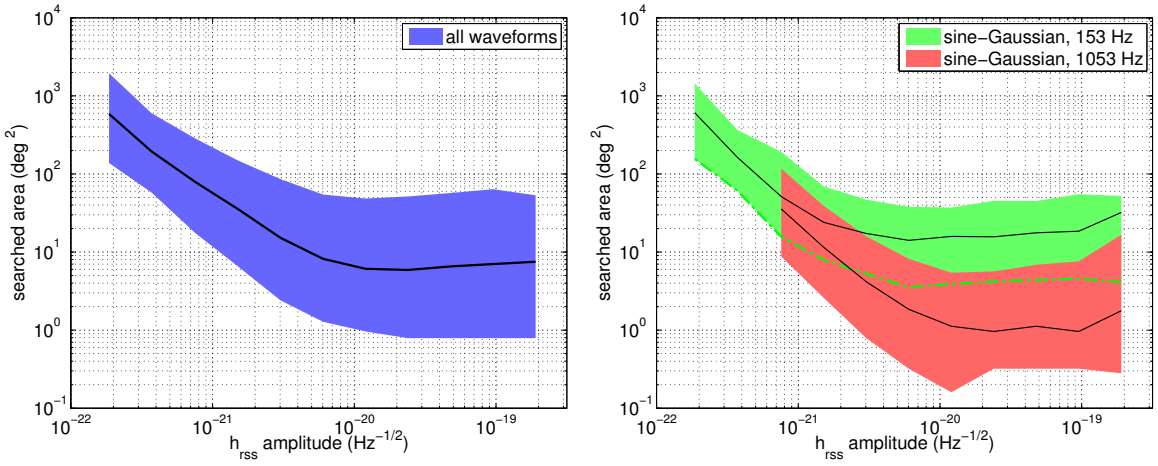

Figure 4: (left) Plot of typical uncertainty region sizes for the burst search, as a function of GW strain amplitude at Earth, for a mix of *ad hoc* Gaussian, sine-Gaussian, and broadband white-noise burst waveforms [12]. The "searched area" is the area of the skymap with a likelihood value greater than the likelihood value at the true source location. The solid line represents the median (50%) performance, while the upper and lower limits of the shaded area show the 75% and 25% quartile values. The detection threshold of $\eta \simeq 6$ corresponds to signal root-sum-square amplitudes ($h_{\mathrm{rss}}^2 = \int [h_+^2 + h_\times^2] dt$) of approximately $h_{\mathrm{rss}} \sim 0.5 \times 10^{-21}\,\mathrm{Hz}^{-1/2}$ to $\sim 2 \times 10^{-21}\,\mathrm{Hz}^{-1/2}$ [11], depending on signal frequency. Median uncertainty regions at these amplitudes are typically between $30\,\mathrm{deg}^2$ and $200\,\mathrm{deg}^2$. (right) Typical uncertainty region sizes for two specific signal models: short-duration Gaussian-modulated sinusoids (sine-Gaussians) with central frequency 153 Hz or 1053 Hz and bandwidths of 17 Hz or 117 Hz. The larger-bandwidth signal is more precisely localized, as expected from the discussion in Sect. 3.1. See [12] for more details.

4 Observing Scenario

In this section we estimate the sensitivity, possible number of detections, and localization capability for each of the observing scenarios laid out in section 2.2. We discuss each future science run in turn and also summarize the results in Table 1.

We estimate the expected number of binary neutron star coalescence detections using both the lower and upper estimates on the BNS source rate density, $10^{-8} - 10^{-5}\,\mathrm{Mpc}^{-3}\,\mathrm{yr}^{-1}$ [28]. Similar estimates may be made for neutron star – black hole (NS-BH) binaries using the fact that the NS-BH range is approximately a factor of 2 larger[2] than the BNS range, though the uncertainty in the NS-BH source rate density is slightly larger [28]. We assume a nominal ρ_c threshold of 12, at which the expected false alarm rate is $10^{-2}\,\mathrm{yr}^{-1}$. However, such a stringent threshold may not be appropriate for selecting candidates triggers for electromagnetic followup. For example, selecting CBC candidates at thresholds corresponding to a higher background rate of $1\,\mathrm{yr}^{-1}$ ($100\,\mathrm{yr}^{-1}$) would increase the number of true signals subject to electromagnetic followup by about 30% (90%). The area localization for these low-threshold signals is only fractionally worse than for the high-threshold population – by approximately 20% (60%). The localization of NS-BH signals is expected to be similar to that of BNS signals.

For typical burst sources the GW waveform is not well known. However, the performance of burst searches is largely independent of the detailed waveform morphology [11], allowing us to quote an approximate sensitive range determined by the total energy E_{GW} emitted in GWs, the central frequency f_0 of the burst, the detector noise spectrum $S(f_0)$, and the single-detector SNR threshold ρ_{det} [29]:

$$D \simeq \left(\frac{G}{2\pi^2 c^3} \frac{E_{\mathrm{GW}}}{S(f_0) f_0^2 \rho_{\mathrm{det}}^2} \right)^{\frac{1}{2}} .$$

In this document we quote ranges using $E_{\mathrm{GW}} = 10^{-2} M_\odot c^2$ and $f_0 = 150\,\mathrm{Hz}$. We note that $E_{\mathrm{GW}} = 10^{-2} M_\odot c^2$ is an optimistic value for GW emission by various processes (see e.g. [10]); for other values the distance reach scales as $E_{\mathrm{GW}}^{1/2}$. We use a single-detector SNR threshold of 8, corresponding to a typical $\rho_c \simeq 12$ and false alarm rates of $\sim 0.3\,\mathrm{yr}^{-1}$. Due to the tail of the low-frequency background-rate-vs.-amplitude distribution in Fig. 3, we see that varying the selection threshold from a background of $0.1\,\mathrm{yr}^{-1}$ ($\rho_c \gtrsim 15$) to even $3\,\mathrm{yr}^{-1}$ ($\rho_c \gtrsim 10$) would increase the number of true signals selected for electromagnetic followup by a factor $(15/10)^3 \sim 3$, though the area localization for low-SNR bursts may be particularly challenging.

The run durations discussed below are in calendar time. Based on prior experience, we can reasonably expect a duty cycle of ∼80% for each instrument after a few science runs. Assuming downtime periods are uncorrelated among detectors, this means 50% coincidence time in a 3-detector network. Our estimates of expected number of detections account for these duty cycles. They also account for the uncertainty in the detector sensitive ranges as indicated in Fig. 1.

4.1 2015 run: aLIGO 40 – 80 Mpc, AdV 20 Mpc

This is envisioned as the first advanced detector science run, lasting three months. The aLIGO sensitivity is expected to be similar to the "early" curve in Fig. 1, with a BNS range of 40 – 80 Mpc and a burst range of 40 – 60 Mpc. The Virgo detector will be in commissioning, but may join the run with a ∼ 20 Mpc BNS range.

[2] This assumes a black hole mass of $10\,M_\odot$.

A three month run gives a BNS search volume[3] of $(0.4-3)\times 10^5\,\mathrm{Mpc}^3\,\mathrm{yr}$ at the confident detection threshold of $\rho_c = 12$. We therefore expect $0.0004-3$ BNS detections. A detection is likely only if the most optimistic astrophysical rates hold.

With the 2-detector H1-L1 network any detected events would not be well localized, and even if AdV joins the run this will continue to be the case due to its lower sensitivity. Follow-up observations of a GW signal would therefore likely rely on localizations provided by another instrument, such as a gamma-ray burst satellite.

4.2 2016–17 run: aLIGO 80 – 120 Mpc, AdV 20 – 60 Mpc

This is envisioned to be a six month run with three detectors. The aLIGO performance is expected to be similar to the "mid" curve in Fig. 1, with a BNS range of 80 – 120 Mpc and a burst range of 60 – 75 Mpc. The AdV range may be similar to the "early" curve, approximately 20 – 60 Mpc for BNS and 20 – 40 Mpc for bursts. This gives a BNS search volume of $(0.6-2)\times 10^6\,\mathrm{Mpc}^3\,\mathrm{yr}$, and an expected number of $0.006-20$ BNS detections. Source localization for various points in the sky for CBC signals for the 3-detector network is illustrated in Fig. 5.

4.3 2017–18 run: aLIGO 120 – 170 Mpc, AdV 60 – 85 Mpc

This is envisioned to be a nine month run with three detectors. The aLIGO (AdV) sensitivity will be similar to the "late" ("mid") curve of Fig. 1, with BNS ranges of 120 – 170 Mpc and 60 – 85 Mpc respectively and burst ranges of 75 – 90 Mpc and 40 – 50 Mpc respectively. This gives a BNS search volume of $(3-10)\times 10^6\,\mathrm{Mpc}^3\,\mathrm{yr}$, and an expected $0.04-100$ BNS detections. Source localization for CBC signals is illustrated in Fig. 5. While the greater range compared to the 2016–17 run increases the expected number of detections, the detector bandwidths are marginally smaller. This slightly degrades the localization capability for a source at a fixed signal-to-noise ratio.

4.4 2019+ run: aLIGO 200 Mpc, AdV 65 – 130 Mpc

At this point we anticipate extended runs with the detectors at or near design sensitivity. The aLIGO detectors are expected to have a sensitivity curve similar to the "design (2019)" curve of Fig. 1. AdV may be operating similarly to the "late" curve, eventually reaching the "design" sensitivity c.2021. This gives a per-year BNS search volume of $2\times 10^7\,\mathrm{Mpc}^3\,\mathrm{yr}$, giving an expected (0.2 - 200) confident BNS detections annually. Source localization for CBC signals is illustrated in Fig. 5. The fraction of signals localized to areas of a few tens of square degrees is greatly increased compared to previous runs. This is due to the much larger detector bandwidths, particularly for AdV; see Fig. 1.

4.5 2022+ run: aLIGO (including India) 200 Mpc, AdV 130 Mpc

The four-site network incorporating LIGO-India at design sensitivity will have both improved sensitivity and better localization capabilities. The per-year BNS search volume increases to $4\times 10^7\,\mathrm{Mpc}^3\,\mathrm{yr}$, giving an expected $0.4-400$ BNS detections annually. Source localization is illustrated in Fig. 5. The addition of a fourth detector site allows for good source localization over the whole sky.

5 Conclusions

We have presented a possible observing scenario for the Advanced LIGO and Advanced Virgo network of gravitational wave detectors, with emphasis on the expected sensitivities and sky local-

[3] The search volume is $\frac{4}{3}\pi R^3\times T$, where R is the range and T the observing time.

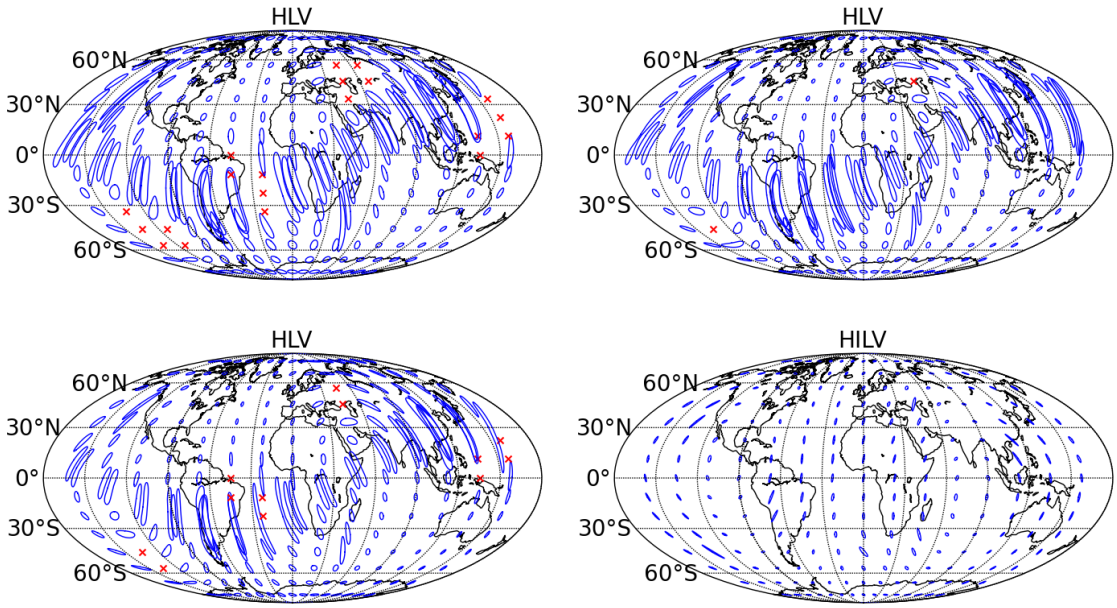

Figure 5: Network sensitivity and localization accuracy for face-on BNS systems with advanced detector networks. The ellipses show 90% confidence localization areas, and the red crosses show regions of the sky where the signal would not be confidently detected. The top two plots show the localization expected for a BNS system at 80 Mpc by the HLV network in the 2016–17 run (left) and 2017–18 run (right). The bottom two plots show the localization expected for a BNS system at 160 Mpc by the HLV network in the 2019+ run (left) and by the HILV network in 2022+ with all detectors at final design sensitivity (right). The inclusion of a fourth site in India provides good localization over the whole sky.

Epoch	Estimated Run Duration	$E_{\rm GW} = 10^{-2} M_\odot c^2$ Burst Range (Mpc)		BNS Range (Mpc)		Number of BNS Detections	% BNS Localized within	
		LIGO	Virgo	LIGO	Virgo		$5\,\mathrm{deg}^2$	$20\,\mathrm{deg}^2$
2015	3 months	40 – 60	–	40 – 80	–	0.0004 – 3	–	–
2016–17	6 months	60 – 75	20 – 40	80 – 120	20 – 60	0.006 – 20	2	5 – 12
2017–18	9 months	75 – 90	40 – 50	120 – 170	60 – 85	0.04 – 100	1 – 2	10 – 12
2019+	(per year)	105	40 – 80	200	65 – 130	0.2 – 200	3 – 8	8 – 28
2022+ (India)	(per year)	105	80	200	130	0.4 – 400	17	48

Table 1: Summary of a plausible observing schedule, expected sensitivities, and source localization with the advanced LIGO and Virgo detectors, which will be strongly dependent on the detectors' commissioning progress. The burst ranges assume standard-candle emission of $10^{-2} M_\odot c^2$ in GWs at 150 Hz and scale as $E_{\rm GW}^{1/2}$. The burst and binary neutron star (BNS) ranges and the BNS localizations reflect the uncertainty in the detector noise spectra shown in Fig. 1. The BNS detection numbers also account for the uncertainty in the BNS source rate density [28], and are computed assuming a false alarm rate of $10^{-2}\,\mathrm{yr}^{-1}$. Burst localizations are expected to be broadly similar to those for BNS systems, but will vary depending on the signal bandwidth. Localization and detection numbers assume an 80% duty cycle for each instrument.

ization accuracies. This network is expected to begin operations in 2015. Unless the most optimistic astrophysical rates hold, two or more detectors with an average range of at least 100 Mpc and with a run of several months will be required for detection.

Electromagnetic followup of GW candidates *may* help confirm GW candidates that would not be confidently identified from GW observations alone. However, such follow-ups would need to deal with large position uncertainties, with areas of many tens to thousands of square degrees. This is likely to remain the situation until late in the decade. Optimizing the EM follow-up and source identification is an outstanding research topic. Triggering of focused searches in GW data by EM-detected events can also help in recovering otherwise hidden GW signals.

Networks with at least 2 detectors with sensitivities of the order of 200 Mpc are expected to yield detections with a year of observation based purely on GW data even under pessimistic predictions of signal rates. Sky localization will continue to be poor until a third detector reaches a sensitivity within a factor of ~ 2 of the others and with a broad frequency bandwidth. With a four-site detector network at final design sensitivity, we may expect a significant fraction of GW signals to be localized to as well as a few square degrees by GW observations alone.

The purpose of this document is to provide information to the astronomy community to facilitate planning for multi-messenger astronomy with advanced gravitational-wave detectors. *While the scenarios described here are our best current projections, they will likely evolve as detector installation and commissioning progresses.* We will therefore update this document regularly.

The authors gratefully acknowledge the support of the United States National Science Foundation for the construction and operation of the LIGO Laboratory, the Science and Technology Facilities Council of the United Kingdom, the Max-Planck-Society, and the State of Niedersachsen/Germany for support of the construction and operation of the GEO600 detector, and the Italian Istituto Nazionale di Fisica Nucleare and the French Centre National de la Recherche Scientifique for the construction and operation of the Virgo detector. The authors also gratefully acknowledge the support of the research by these agencies and by the Australian Research Council, the International Science Linkages program of the Commonwealth of Australia, the Council of Scientific and Industrial Research of India, the Istituto Nazionale di Fisica Nucleare of Italy, the Spanish Ministerio de Educación y Ciencia, the Conselleria d'Economia Hisenda i Innovació of the Govern de les Illes Balears, the Foundation for Fundamental Research on Matter supported by the Netherlands Organisation for Scientific Research, the Polish Ministry of Science and Higher Education, the FOCUS Programme of Foundation for Polish Science, the Royal Society, the Scottish Funding Council, the Scottish Universities Physics Alliance, The National Aeronautics and Space Administration, the Carnegie Trust, the Leverhulme Trust, the David and Lucile Packard Foundation, the Research Corporation, and the Alfred P. Sloan Foundation. This document has been assigned LIGO Document number P1200087, Virgo Document number VIR-0288A-12.

References

[1] Harry, G. M. for the LIGO Scientific Collaboration. *Classical and Quantum Gravity* **27**, 084006 (2010).

[2] Acernese, F. et al. Virgo Technical Report VIR-0027A-09 (2009), https://tds.ego-gw.it/ql/?c=6589.

[3] Accadia, T. et al. Virgo Document VIR-0128A-12 (2012), https://tds.ego-gw.it/ql/?c=8940.

[4] Abadie, J. et al. LIGO Document number T1200286-v3 (2012), https://dcc.ligo.org/LIGO-T1200286-v3/public.

[5] Abadie, J. et al. LIGO Document number M1200055-v2, Virgo Document number VIR-0173A-12 (2012), https://dcc.ligo.org/LIGO-M1200055-v2/public.

[6] Finn, L. S. and Chernoff, D. F. *Phys. Rev. D* **47** 2198–2219 (1993), arXiv:9301003 [gr-qc].

[7] Lück, H. et al. *J. Phys.: Conf. Ser.* **228** 012012 (2010), arXiv:1004.0339.

[8] Somiya, K. *Classical and Quantum Gravity* **29** 124007 (2012), arXiv:1111.7185.

[9] Abadie, J. et al. *Phys. Rev. D* **85** 082002 (2012), arXiv:1111.7314.

[10] Abadie, J. et al. *Astrophys.J.* **760** 12 (2012), arXiv:1205.2216.

[11] Abadie, J. et al. *Phys. Rev. D* **85** 122007 (2012), arXiv:1202.2788.

[12] Abadie, J. et al. *Astronomy & Astrophysics* **539** A124 (2012), arXiv:1109.3498.

[13] Abadie, J. et al. *Astronomy & Astrophysics* **541** A155 (2012), arXiv:1112.6005.

[14] Evans, P. A. et al. *Astrophys.J. Supplements* **203** 28 (2012), arXiv:1205.1124.

[15] Fairhurst, S. *New J.Phys.* **11** 123006 (2009), arXiv:0908.2356.

[16] Fairhurst, S. *Class.Quant.Grav.* **28** 105021 (2011), arXiv:1010.6192.

[17] Vitale, S. and Zanolin, M. *Phys. Rev. D* **84** 104020 (2011), arXiv:1108.2410.

[18] Vitale, S. et al. *Phys.Rev.* **D85** 064034 (2012), arXiv:1111.3044.

[19] Nissanke, S., Sievers, J., Dalal, N., and Holz, D. *Astrophys.J.* **739** 99 (2011), arXiv:1105.3184.

[20] Veitch, J. et al. *Phys. Rev. D* **85** 104045 (2012), arXiv:1201.1195.

[21] Nissanke, S., Kasliwal, M., and Georgieva, A. arXiv:1210.6362.

[22] Chatterji, S. et al. *Phys.Rev.* **D74** 082005 (2006), arXiv:0605002 [gr-qc].

[23] Dimmelmeier, H., Ott, C. D., Marek, A., and Janka, H.-T. *Phys. Rev. D* **78** 064056 (2008).

[24] Ott, C. D. *Class. Quantum Grav.* **26** 063001 (2009), arXiv:0809.0695.

[25] Yakunin, K. N. et al. *Classical and Quantum Gravity* **27** 194005 (2010), arXiv:1005.0779.

[26] Ott, C. D. et al. *Physical Review Letters* **106** 161103 (2011), arXiv:1012.1853.

[27] Klimenko, S. et al. *Physical Review D* **83** 102001 (2011), arXiv:1101.5408.

[28] Abadie, J. et al. *Classical and Quantum Gravity* **27** 173001 (2010), arXiv:1003.2480.

[29] Sutton, P. J. arXiv:1304.0210.